ROYAL SOCIETY
OF CHEMISTRY

PAPER

Check for updates

Effects of Bi and Sb ion incorporation on the optoelectronic properties of mixed lead–tin perovskites†

F. M. Rombach, [ID] [a] L. Gregori, [bh] A. Sidler, [c] J. Whitworth, [d] S. Zeiske, [ef] H. Jin, [a] E. Y-H. Hung, [ID] [a] S. Motti, [ID] [g] P. Caprioglio, [a] A. Armin, [ID] [e] M. Lenz, [ID] [cj] D. Meggiolaro,*[h] F. De Angelis[bhi] and H. J. Snaith [ID] *[a]

Doping with small densities of foreign ions is an essential strategy for tuning the optoelectronic properties of semiconductors, but the effects of doping are not well-understood in halide perovskites. We investigate the effect of Bi^{3+} and Sb^{3+} doping in lead–tin perovskites. Films doped with small amounts of BiI_3 and SbI_3 show greatly increased non-radiative recombination at precursor doping concentrations as low as 1 ppm for Bi^{3+} and 1000 ppm for Sb^{3+}. We rationalize such behaviour by density functional theory (DFT) simulations, showing that these metal ions can be incorporated in the perovskite crystal by introducing deep trap levels in the band gap. Having found that very small amounts of Bi^{3+} greatly reduce the optoelectronic quality of lead–tin perovskite films, we investigate the presence of Bi impurities in perovskite precursor chemicals and find quantities approaching 1 ppm in some. In response, we introduce a facile method for removing Bi^{3+} impurities and demonstrate removal of 100 ppm Bi from a perovskite ink. This work demonstrates how the incorporation of small concentrations of foreign metal ions can severely affect film quality, raising the importance of precursor chemical purity.

[a] *Department of Physics, University of Oxford, Clarendon Laboratory, Parks Road, Oxford, OX1 3PU, UK. E-mail: henry.snaith@physics.ox.ac.uk*

[b] *Department of Chemistry, Biology and Biotechnology, University of Perugia and INSTM, Via Elce di Sotto 8, 06123, Perugia, Italy*

[c] *Institute for Ecopreneurship, School of Life Sciences, University of Applied Sciences and Arts Northwestern Switzerland, Hofackerstrasse 30, 4132 Muttenz, Switzerland*

[d] *Materials Innovation Factory, University of Liverpool, 51 Oxford Street, Liverpool L7 3NY, UK*

[e] *Sustainable Advanced Materials (Sêr-SAM), Centre for Integrative Semiconductor Materials and Department of Physics, Swansea University Bay Campus, Fabian Way, Swansea, SA1 8EN, UK*

[f] *Department of Chemistry, Northwestern University, Evanston, IL 60208, USA*

[g] *School of Physics and Astronomy, Faculty of Engineering and Physical Sciences, University of Southampton, University Road, Southampton SO17 1BJ, UK*

[h] *Computational Laboratory for Hybrid/Organic Photovoltaics (CLHYO), Istituto CNR di Scienze e Tecnologie Chimiche "Giulio Natta" (CNR-SCITEC), Via Elce di Sotto 8, Perugia, 06123, Italy. E-mail: daniele.meggiolaro@cnr.it*

[i] *SKKU Institute of Energy Science and Technology (SIEST), Sungkyunkwan University, Suwon, 440-746, Korea*

[j] *Department of Environmental Technology, Wageningen University, Wageningen 6708 WG, the Netherlands*

† Electronic supplementary information (ESI) available. See DOI: https://doi.org/10.1039/d4tc02162b

1. Introduction

Lead halide perovskites (LHP) are outstanding materials for photovoltaics due to their excellent optoelectronic properties, such as direct band gaps, high absorption coefficients and long charge carrier lifetimes and diffusion lengths.[1] The partial replacement of lead with tin narrows the band gap of the perovskite from 1.6 to ∼1.2 eV for lead–tin ratios around 40/60.[2,3] Mixed lead–tin perovskites are thus promising materials for the development of single-junction as well as all-perovskite tandem solar cells in combination with neat LHPs.[4]

Compared to LHPs, however, mixed lead–tin perovskites experience increased self-p-doping that may hinder their efficiencies in solar cells. When the amount of tin is comparable to lead, background hole densities in the range 10^{14}–10^{17} cm^{-3} are reported.[5–7] Such a wide range of reported values can be explained by variations in processing conditions between labs, particularly the extent of oxygen exposure before and during film deposition, which can strongly affect the density of Sn^{2+} vacancies. The increase in p-doping when moving from a lead-dominant to a tin-dominant perovskite composition is mainly due to a shift in the energy of the perovskite valence band maximum (VBM) towards the vacuum level, inducing a stabilization of the acceptor defects in the material. In parallel, the

This journal is © The Royal Society of Chemistry 2025

J. Mater. Chem. C, 2025, **13**, 5161–5171 | **5161**

facile oxidation of tin(II) to tin(IV) promotes the formation of tin vacancies, limiting the long-term stability of the material.[8,9]

The ability to control the long-term stability and the self-p-doping level is of central importance for the full exploitation of lead–tin perovskites in solar cells. Reducing the background hole density below 10^{15} cm^{-3} is expected to improve energetic alignment,[10] as well as reduce loss pathways involving the recombination of photo-excited electrons with the hole background.[11] The use of SnF$_2$ and Sn metal additives has been shown to successfully limit tin oxidation and the incorporation of Sn^{4+} during the perovskite film deposition.[7,12,13] However, the magnitude by which these strategies can reduce self-p-doping in Sn-based perovskites is limited.[12]

Shifting the Fermi level of halide perovskites has been found to be surprisingly challenging compared to other semiconductor materials.[14] Whilst both intrinsic doping (by under- or over-stoichiometric precursor ratios) and extrinsic doping (by the introduction of lattice impurities) have been successfully used to somewhat increase background carrier densities, large shifts in Fermi level remain elusive. Theoretical investigation suggests that this is mainly due to the facile formation of compensatory intrinsic defects in perovskite in response to doping, and the difficulty in finding dopants with formation energies of their presence in the lattice much smaller than the most stable structural defect.[15]

One strategy to control the p-doping and possibly increase the stability of lead–tin perovskites while retaining the native band gap is doping with metal ions. The incorporation of these ions may move the Fermi level in these materials by both directly introducing free carriers by ionization or by affecting the formation energies of intrinsic defects, inducing a shift in defect chemistry. Previously, heterovalent metal dopants such as Rb$^+$, K$^+$, Na$^+$, Ga^{3+} and Ag$^+$ have been demonstrated to increase the formation energies of Sn vacancies and passivate I$^-$ vacancies or iodine trimers, reducing non-radiative recombination rates in a range of perovskite compositions.[16–21] There have also been previous experimental indications that the background carrier density of perovskites may be modulated through doping, e.g. by Ga^{3+} in lead–tin perovskites,[18] and Bi^{3+} in neat lead perovskites.[22] A challenge associated with doping is that metal ions much smaller or larger than Sn^{2+}/Pb^{2+} are unlikely to be incorporated in the lattice at significant densities,[22,23] be incorporated preferentially at interfaces,[18] or even migrate out of the perovskite structure over time, reversing the effects of doping.[17] In addition to this, the charge imbalance introduced by the incorporation of heterovalent dopants is expected to be partially compensated by the formation of negatively charged defects such as Pb^{2+} vacancies, A-cation vacancies or I$^-$ interstitials,[18,22] which will not only decrease doping efficiency but may also negatively impact optoelectronic properties. Hence, the impact of metal dopants on the Fermi level of halide perovskites depends not only upon their ionization energy, but also on their effect on the formation energies of native perovskite defects.

Due to the comparable ionic radius and the similar electronic structure, Bi and Sb metals appear as a natural choice for n-doping, and hence compensate the self-p-doping and increasing the lattice stability of lead–tin perovskites. They are suggested to n-dope by incorporating in the perovskite in their 3+ charge state.[24,25] Previous experimental works, however, have highlighted the emergence of deep trap states associated with the Bi^{3+} dopant in neat lead perovskites, strongly impacting the optoelectronic properties by increased non-radiative recombination.[26–29] Such observations are in agreement with theoretical predictions.[24,25] Recent computational studies on neat-Sn perovskite compositions found both Bi and Sb introduce deep recombination levels even when lead was entirely substituted by Sn.[30] The deep ionization levels associated with the dopants shift down in energy by moving from lead to tin perovskite, keeping their deep nature. This is mainly due to the increase in energy of the VBM of the perovskite moving from lead to tin. A recent investigation on the effects of relatively large concentrations of Bi doping (1+%) of mixed lead–tin perovskites found that Bi also induces increased non-radiative recombination in these materials. Although Sb^{3+} doping has also been indicated to slightly n-dope neat lead perovskites, it has not been as widely explored.[31,32] The effects of small densities of both Bi^{3+} and Sb^{3+} doping on lead–tin perovskites hence remain unexplored.
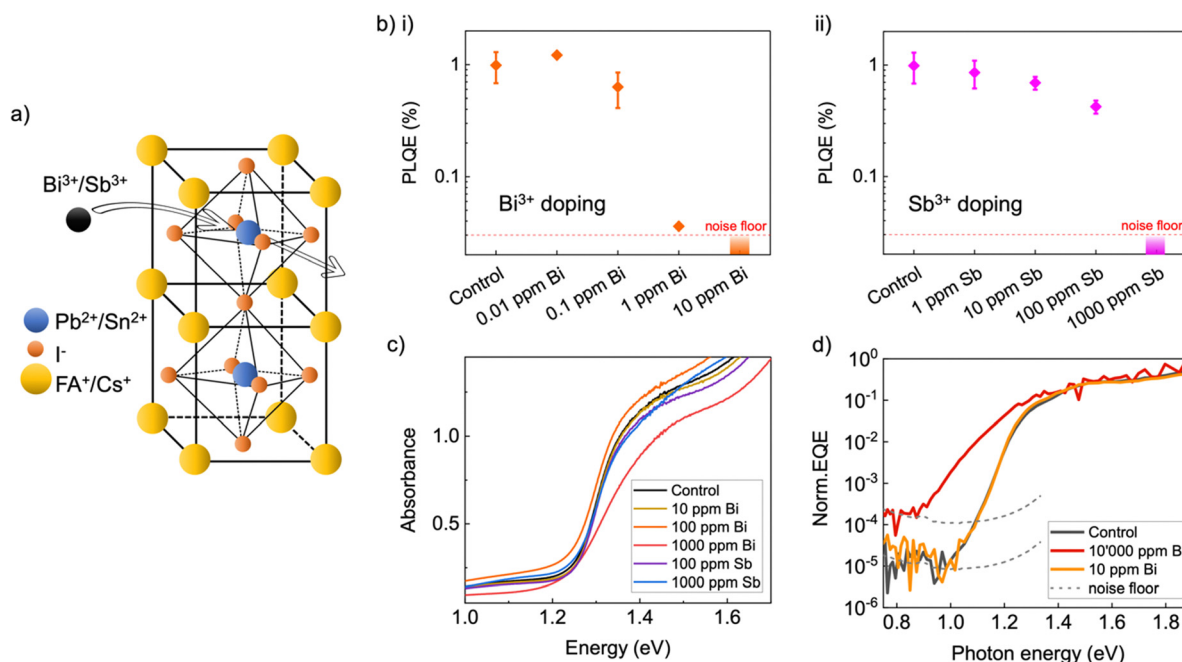
In this work we investigate the impact of Bi^{3+} and Sb^{3+} metal dopants on the optoelectronic properties of mixed lead–tin perovskites. We explore a wide range of dopant concentrations down to 0.01 ppm and find that Bi^{3+} doping densities as low as 1 ppm (corresponding to a Bi^{3+} density of $\sim 10^{15}$ cm^{-3} in the film) severely quench the photoluminescence of the perovskite. Sb^{3+} doping is also found to quench photoluminescence, but only at significantly higher densities of 100 ppm. The observed increase in non-radiative recombination is rationalized using DFT simulations. These show that both Bi^{3+} and Sb^{3+} can incorporate into the lattice of lead–tin perovskites, but induce deep electron traps in the band gap, similarly to what has been previously observed in neat lead perovskites. The disastrous impact of very small amounts of Bi^{3+} on the optoelectronic quality of the perovskite poses serious concerns regarding its presence as a potential impurity in perovskite precursor chemicals. Motivated by this, we carried out chemical impurity analysis of different precursor powders and found that in some precursors Bi is present in amounts that could affect perovskite quality. In response, we develop and validate a strategy to remove Bi^{3+} impurities from perovskite precursor chemicals based on reduction by Sn^0 metal.

2. Results & discussion

2.1 Optoelectronic quality of Bi^{3+} and Sb^{3+}-doped lead–tin perovskite films

To investigate the effects of Bi^{3+} and Sb^{3+} doping on the optoelectronic properties of mixed lead–tin perovskites, we fabricated perovskite films with 0.001 ppm (10^{-7}% in the precursor solution, or 1×10^{12} cm^{-3} in the films) to 50 000 ppm (5%, or 5×10^{19} cm^{-3}) dopant. Films were doped by adding BiI$_3$ and SbI$_3$ (from stock solutions) to the filtered

5162 | *J. Mater. Chem. C*, 2025, **13**, 5161–5171

This journal is © The Royal Society of Chemistry 2025

Fig. 1 (a) Schematic illustrating trivalent doping of hybrid lead–tin perovskites. Bi^{3+} or Sb^{3+} incorporate at the substitutional Pb^{2+} site. The partial charge compensation by the formation of Sn^{2+}/Pb^{2+} vacancies is also illustrated. (b) PLQE of lead–tin perovskite films doped with small quantities of (i) Bi^{3+} or (ii) Sb^{3+}. (c) Absorbance around the band edge of lead–tin perovskite films doped with various amounts of Bi^{3+} and Sb^{3+}. (d) Ultra-sensitive EQE measurements of electrically contacted lead–tin perovskite films doped with various amounts of Bi^{3+}.

perovskite precursor solution, after which the precursor was stirred for 60 minutes. As SbI_3 was found to be less soluble in these solvents, it could only be investigated up to a doping density of 1000 ppm (0.1%, or 1×10^{18} cm^{-3}). The higher concentrations of Bi^{3+} and Sb^{3+} caused a clear reddish discoloration of the perovskite precursor solution. Bi^{3+} and Sb^{3+} are expected to be incorporated into the perovskite lattice at the metal cation position (Fig. 1a). Although the dopant added to the precursor solution may not entirely incorporate in the perovskite bulk at the higher concentrations, we expect that the density of incorporated dopant will follow the trend of dopant precursor concentration. For example, for Bi doping of $MAPbBr_3$ it has been shown that Bi is incorporated into the lattice at approximately the same concentration as $BiBr_3$ in the perovskite precursor solution.[28] Throughout our paper, references to dopant density refer to the concentration of dopant added to the perovskite precursor solution, with respect to the sum of the lead and tin concentrations.

Perovskite thin films were successfully deposited by solution processing from precursors containing the Bi^{3+} and Sb^{3+} doping densities described, with no significant visible differences in film drying and curing. We characterized these films by X-ray diffraction (XRD) (Fig. S1, ESI†) and found that the original lead–tin perovskite phase is unchanged for all concentrations of Bi^{3+} and Sb^{3+} tested. Optical measurements of both Bi^{3+} and Sb^{3+}-doped films confirm this by showing no shift in band gap for the full range of doping densities. We did observe a slight reduction in XRD scattering peak intensity at Bi^{3+} densities above 5000 ppm. When 50 000 ppm Bi^{3+} was added, we also observed two new XRD peaks corresponding to BiI_3, suggesting that at this precursor concentration there is a significant amount of excess Bi^{3+} which is not incorporated in the

perovskite crystal. This is consistent with previous studies on single crystals of Bi doped $MAPbBr_3$, where Bi incorporation could be observed up to around 50 000 ppm doping.[27,28]

To map the effect of Bi^{3+} and Sb^{3+} doping on the optoelectronic quality of the lead–tin perovskite films, we performed steady-state photoluminescence quantum efficiency (PLQE) measurements. Samples were excited with a red 660 nm laser at an intensity which resulted in an absorbed photon flux equivalent to AM 1.5 1 sun conditions for a 1.25 eV bandgap material. Surprisingly, we found that very small amounts of Bi^{3+} doping led to a severe decrease in the PLQE of the lead–tin perovskite films (Fig. 1b(i)), with the addition of 1 ppm Bi^{3+} causing an ∼80% reduction in PLQE with respect to undoped samples. To confirm, we also performed time-resolved photoluminescence (TRPL) decay measurements on the same samples and fitted the tails of the decays with a mono-exponential decay (Fig. S2, ESI†). The dynamics show an identical trend to the PLQE, with 1 ppm Bi^{3+} causing a ∼10-fold decrease in lifetime with respect to controls. This suggests that the addition of even very small densities of Bi^{3+} severely increases the rate of non-radiative recombination in PbSn perovskites. This is consistent with previous observations of Bi^{3+} doping in neat lead perovskites, in which 10 ppm Bi^{3+} was observed to already reduce device performance.[26]

Doping the lead–tin perovskite in the same manner with Sb^{3+} revealed that this dopant similarly increases non-radiative recombination rates in the perovskite films, but at significantly higher concentrations of 100–1000 ppm (Fig. 1b(ii)). For doping densities that did not completely quench the photoluminescence (below 1 ppm for Bi^{3+} and 1000 ppm for Sb^{3+}), we found no change in either the position or the shape of the PL

This journal is © The Royal Society of Chemistry 2025

J. Mater. Chem. C, 2025, **13**, 5161–5171 | **5163**

emission peak (Fig. S3, ESI†). Whilst previous investigations of Bi^{3+} doping in $MAPbBr_3$ observed an enhanced emission in the region of 1000–1080 nm in the doped films,[27–29] we did not observe any new emission peaks at longer wavelengths up to our detector limit of 1400 nm.

We could not discern significant changes to the above band-gap absorption properties, as measured by UV-vis-NIR transmission and reflectance spectrophotometry (Fig. 1c). To probe more subtle changes that may occur in the sub-bandgap region of the absorption onset and tail, we performed ultra-sensitive external quantum efficiency (EQE) measurements on electrically contacted Bi^{3+}-doped lead–tin perovskite films.[33] Films doped with 10 000 ppm Bi^{3+} show a significant broadening of the EQE onset (Fig. 1d). This can be ascribed to increased energetic disorder, which has previously also been observed by others in Bi^{3+}-doped neat Pb perovskites.[26–29] However, for films doped with 10 ppm Bi^{3+}, both EQE and absorptance spectra were found to be very similar to films without any Bi^{3+}, despite the PLQE being strongly quenched at this density. Analogously, we also observed no change in the absorptance spectra of Sb^{3+}-doped films up to 1000 ppm density. Hence, we conclude that at impurity levels between 1–10 ppm for Bi^{3+} and above 100 ppm for Sb^{3+}, doping with these elements does not affect electronic disorder to an observable extent but does significantly increase the rate of non-radiative recombination. This would be consistent with the Bi^{3+} and Sb^{3+} dopants creating highly recombination-active traps in the perovskite, which cause rapid recombination even at densities that do not observably increase electronic disorder.

2.2 DFT simulations

To rationalize the observed impact of Bi^{3+} and Sb^{3+} on the lead–tin perovskite, we investigated the efficacy of their incorporation and their effect on the electronic band structure and defect energies of $MAPb_{0.5}Sn_{0.5}I_3$ through DFT calculations. For simplicity, we have chosen MA as the mono-valent cation for the DFT calculations. Since the band structure near the CB minimum and VB maxima are dominated by the divalent metal and halide orbitals, and the crystal structure and lattice constant of a formamidinium/cesium mixed cation perovskite is similar to the MA perovskite, we do not expect that the choice of monovalent cation will significantly influence the calculated defect energies induced by the group V metal doping. Dopant equilibrium structures were obtained by using the Perdew–Burke–Ernzherof (PBE) functional[34] in the $2 \times 2 \times 2$ supercell of the phase with densities of $\sim 3\%$, see Computational details in ESI.†

As expected, DFT analysis highlights that the incorporation of the dopants is thermodynamically more favorable in substitutional position to Pb and Sn than other positions in the lattice, *e.g.* interstitial or substitutional to the organic cation (see Table S1 of ESI†). Furthermore, the incorporation in substitutional position to Pb is slightly more favorable than on the Sn site for both Bi and Sb (see Table S1 and Fig. S4, ESI†), due to the more similar ionic radius of the dopants with lead. Hence, our defect analysis has been focused on dopants in substitutional position to Pb in the lattice. To provide accurate defect properties, the defect formation energies and thermodynamic ionization levels (TIL) have been calculated by using the PBE0 hybrid functional ($\alpha = 0.20$)[35,36] and by including spin–orbit coupling (SOC), see Computational details.

In Fig. 2a the calculated defect formation energies of the substitutional dopants in I-medium conditions of growth are reported and compared to defect formation energies of the most stable native defects in $MAPb_{0.5}Sn_{0.5}I_3$, *i.e.* V_{Pb}^{2-}, V_{Sn}^{2-}, I_i^- and V_I^+. Bi dopant is stable in the positive state of charge (+III oxidation state) for Fermi levels up to 0.52 eV, where a deep (+/0) transition is present and the neutral state becomes the
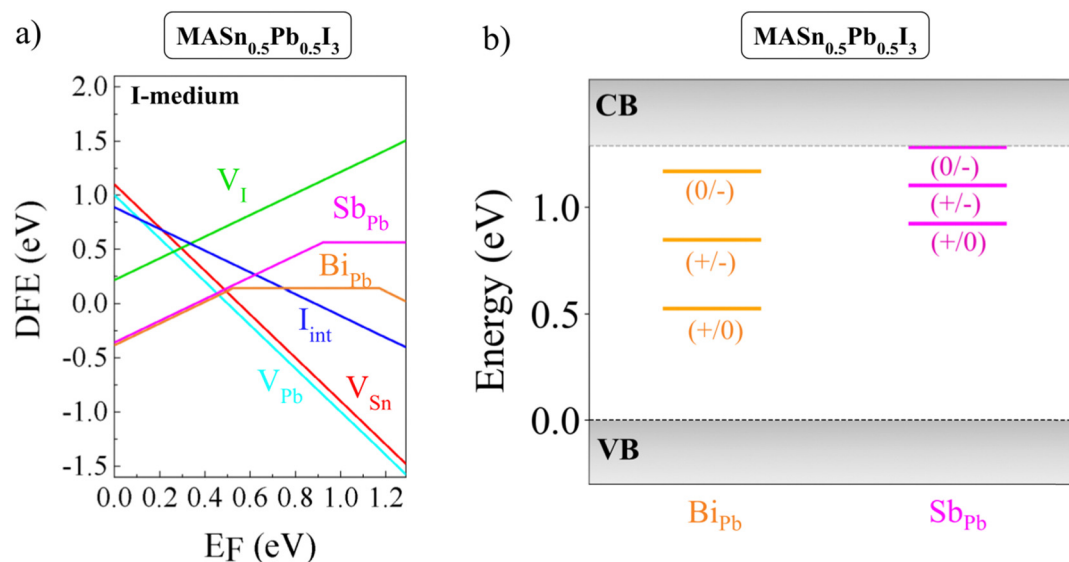

Fig. 2 (a) Defect formation energies of substitutional Bi_{Pb} and Sb_{Pb} dopants compared with the more stable native defects in $MAPb_{0.5}Sn_{0.5}I_3$ (I-medium conditions); (b) associated thermodynamic ionization levels. Defect quantities have been calculated at PBE0-SOC ($\alpha = 0.20$) level of theory by including DFT-D3 dispersions.
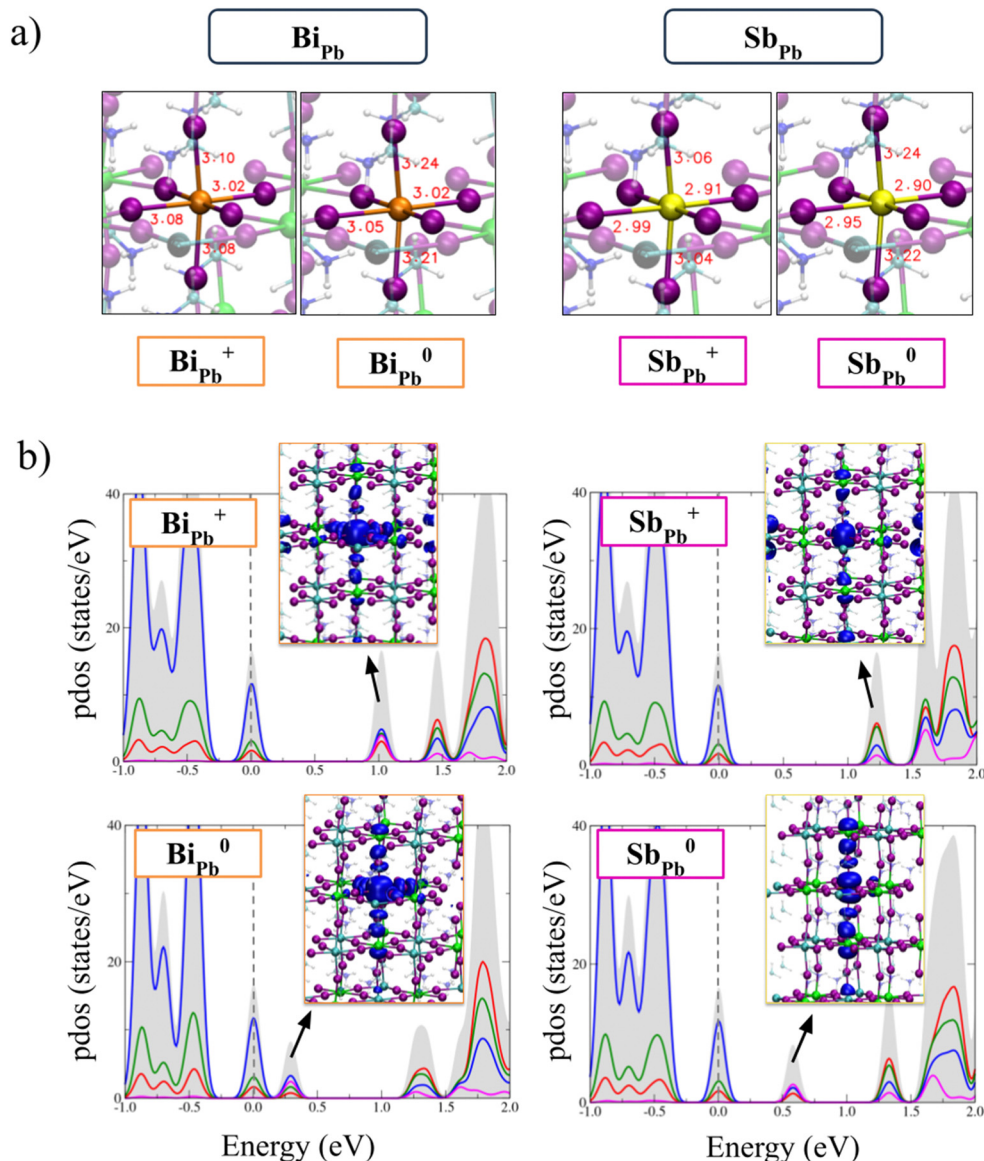
5164 | *J. Mater. Chem. C*, 2025, **13**, 5161–5171

This journal is © The Royal Society of Chemistry 2025

Fig. 3 (a) Equilibrium structures of the positive and neutral Bi_{Pb}, Sb_{Pb} defects; (b) atom-projected density of states (PDOS) of the same defects, highlighting the presence of deep trap states in the band gap of the perovskite (blue = I, red = Pb, green = Sn, purple = dopant). In the diagrams the VBM energy is set to zero (dotted line). In the insets the plots of the LUMO (HOMO) Kohn–Sham (KS) orbitals of the positive (neutral) defects are reported.

stable form of the defect. In heavily n-doped perovskites (Fermi level close to the conduction band) the negative form of the defect is also stable. Due to the similar ionic radius of Bi^{3+} (103 pm) and Pb^{2+} (119 pm), Bi^{3+} incorporation in the Pb site leads to a limited metal–iodide bond variation with respect to the pristine perovskite (see Fig. 3a). The analysis of the projected density of states (PDOS) of Bi_{Pb}^{+} shows that the dopant introduces a localized Kohn–Sham (KS) level in the band gap of the perovskite placed at ~ 1.0 eV above the VBM (see Fig. 3b). Such a state traps one electron upon photoexcitation leading to an occupied KS level placed at 0.3 eV above the VBM, after lattice relaxation (Fig. 3b). Upon the relaxation, an elongation of the Bi–I bond lengths is observed due to the population of the antibonding state of the metal.

The in-gap nature of the LUMO state suggests that no barriers to the trapping of the electron on the Bi_{Pb}^{+} defect are

present. We have investigated the non-radiative recombination of the hole on the neutral Bi_{Pb}^{0} defect by calculating the energy-coordinate diagram of the neutral and positive defect along distortion of the Bi–I bond, see Fig. S7 of ESI.† We have highlighted in the diagram, the presence of a small barrier (0.18 eV) to the recombination of the hole. This indicates that the inclusion of Bi strongly increases electron trapping and subsequent non-radiative recombination in the material.

Compared to Bi, Sb is stable in the +III oxidation state in a wider Fermi level range, with the positive charged state being the most stable form of the defect up to 0.92 eV above the VBM, i.e. the position of the (+/0) deep transition, see Fig. 2. Similarly to Bi, Sb is preferentially incorporated in the +III oxidation state in thermodynamic equilibrium, i.e. Sb_{Pb}^{+}. Due to the smaller radius, Sb^{3+} introduces a slight contraction of the metal–iodide

This journal is © The Royal Society of Chemistry 2025

J. Mater. Chem. C, 2025, 13, 5161–5171 | 5165

bonds, see Fig. 3. The analysis of the electronic structure of the Sb_{Pb}^{+} defect highlights the presence of an unoccupied orbital below the CBM that after the electron trapping leads to the formation of an occupied KS level placed at ~ 0.6 eV above the VBM, as reported in the PDOS of the neutral charged state

(Fig. 3). The (+/0) ionization level of Sb occurs at higher energy with respect to Bi, *i.e.* 0.9 eV *vs.* 0.5 eV above the VBM, highlighting that Sb is a less active charge trap compared to Bi. Notably, the different behavior is attributed to the more limited SOC effects on the p-orbitals of the Sb with respect to Bi, since
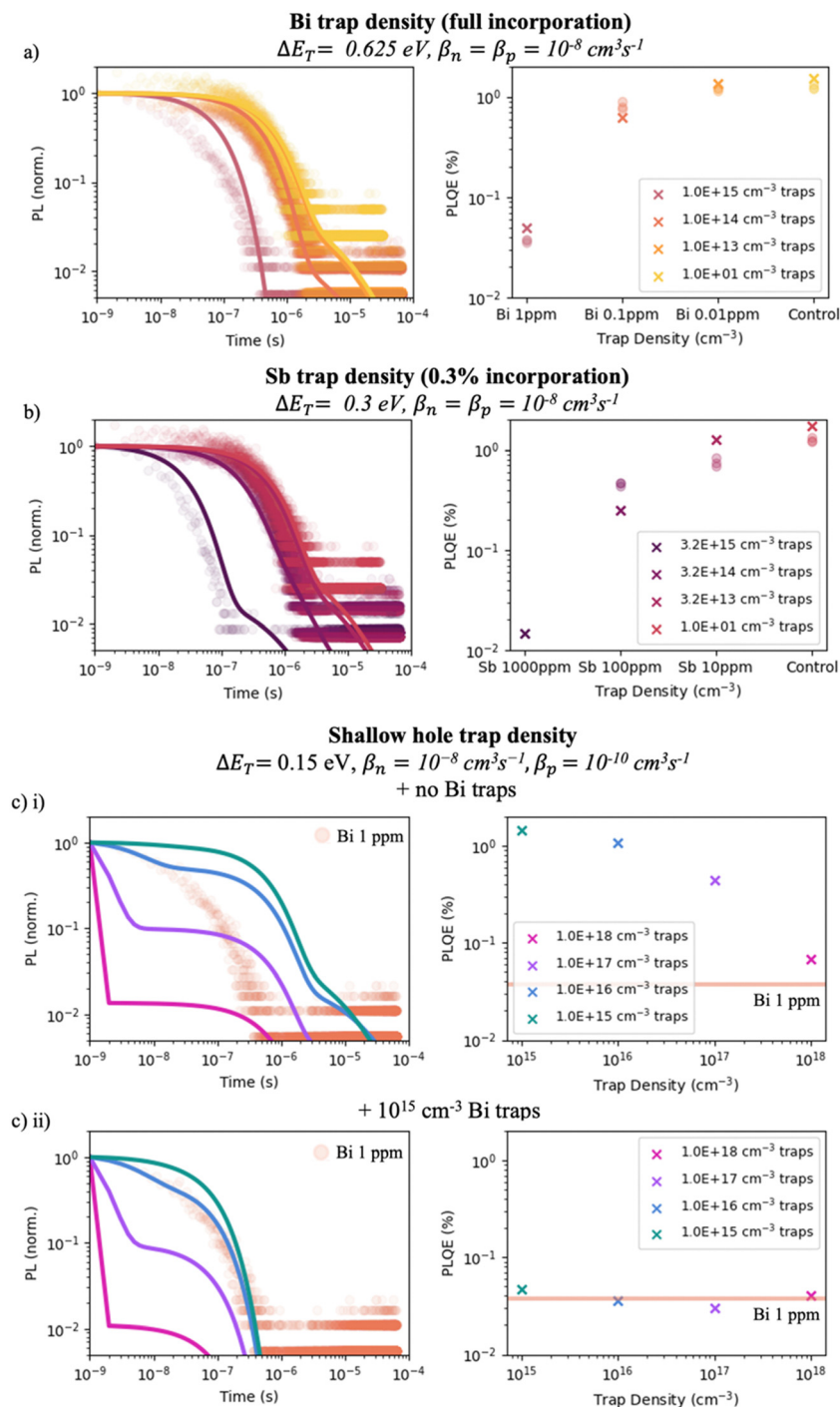
Fig. 4 Simulated TRPL decays and PLQE values with varying trap types and densities. TRPL and PLQE variation with (a) Bi trap density variation (0.625 eV from CB, equal hole and electron capture coefficients of 10^{-8} cm^3 s^{-1}), (b) Sb trap density variation (0.3 eV from CB, equal hole and electron capture coefficients of 10^{-8} cm^3 s^{-1}), and (c) shallow hole trap such as $V_{Pb/Sn}^{2-}$ or I_i^{-} variation (0.15 eV from CB, asymmetrical hole and electron capture coefficients of 10^{-8}, 10^{-10} cm^3 s^{-1} respectively) (i) without additional Bi traps and (ii) with 10^{15} cm^{-3} additional Bi traps. All additional simulation parameters are given in the methods.

5166 | *J. Mater. Chem. C*, 2025, **13**, 5161–5171

This journal is © The Royal Society of Chemistry 2025

without inclusion of relativistic effects the energy difference between the (+/0) transitions in the two cases is around 0.1 eV, see Fig. S4 of ESI.†

In principle, the defect equilibrium obtained after the incorporation of the dopants could have an impact on the charge carrier equilibrium density. In the pristine perovskite the native Fermi level is placed at around 0.3 eV above the VBM and it is mainly set by the equilibrium between iodine vacancies and lead vacancies. After the incorporation of Bi and Sb the DFT calculations predict that the Fermi level shifts by 0.2 eV towards the middle of the band gap, with a decrease in hole density of around four orders of magnitude. If there were no other consequences of the Bi or Sb doping, this significant Fermi level shift would be advantageous.

If completely incorporated in the perovskite structure, the addition of 1 ppm Bi^{3+} would lead to a trap state density of 10^{15} cm^{-3} (substituting 0.0001% of the 10^{21} cm^{-3} Pb/Sn sites in the perovskite lattice). To investigate whether such a density of deep defects can completely explain the observed increase in non-radiative recombination, we performed TRPL and PLQE simulations which are presented in Fig. 5. We find that when modelling Bi as a mid-gap trap (0.625 eV from CB) with symmetrical hole and electron capture coefficients of 10^{-8} cm^{-3} s^{-1}, a density of 10^{15} cm^{-3} (equivalent to the full incorporation of 1 ppm Bi) can indeed closely replicate the reductions in PLQE and TRPL lifetimes observed in the films, with only a slight deviation in the early-time shape of the TRPL decay.

However, performing the same simulation with a shallower trap (0.35 eV from the CB) to simulate the effect of Sb doping shows that the shallower energy level of Sb in the perovskite lattice cannot completely explain the reduced impact on non-radiative recombination (Fig. 4b). We find that the TRPL and PLQE results can be well-reproduced when assuming that only 0.3% of the added Sb incorporates in the perovskite lattice. Alternatively, the electron and hole capture coefficients of the Sb defect may in reality be lower than estimated here. Based on DFT predictions, no remarkable differences in the incorporation energies of Bi and Sb have been observed. Hence, the less severe effect of Sb^{3+} doping on non-radiative recombination rates and energetic disorder may be explained by a combination of a shallower trap energy and a kinetic hindrance to the incorporation of Sb^{3+} ions which are more strongly solvated with respect to Bi^{3+} in the precursor solution.

Defect formation energy analysis confirms that the incorporation of Bi and Sb is largely compensated by the formation of lead or tin vacancies $V_{Pb/Sn}^{2-}$, while the formation of compensating iodine interstitials I_i^- shows more unfavorable thermodynamics, see Table 1. Previous computational studies on neat-lead perovskites demonstrated that non-radiative recombination on the Bi_{Pb}^+ defect is hindered by the presence of a thermodynamic barrier to recombination. The loss of performance of Bi-doped perovskite solar cells was instead attributed to Fermi level shift induced by the dopant, increasing the density of deep acceptor defects, i.e. iodine interstitials, in the material.[37] Whilst we expect Bi doping to cause a similarly large increase in the $V_{Pb/Sn}^{2+}$ and I_i^- acceptor defects here, both of

Table 1 Simulated incorporation reactions of Bi and Sb dopants into the $MAPb_{0.5}Sn_{0.5}I_3$ perovskite and associated thermodynamics calculated at the PBE0-SOC level of theory

Reaction	M = Bi (eV)	M = Sb (eV)
(R1) $3/2Pb_{Pb} + MI_3 \rightarrow M_{Pb}^+ + 1/2V_{Pb}^{2-} + 3/2PbI_2$	0.12	0.14
(R2) $Pb_{Pb} + MI_3 \rightarrow M_{Pb}^+ + I_i^- + PbI_2$	0.50	0.53

these defects were previously calculated to be relatively shallow defects in the bulk of mixed lead–tin perovskites, with a distance from the VB not exceeding 0.15 eV.[8] We hence presume that their recombination activity is limited. To test the effect of an increase in the density of these shallow defects, we simulated their effect on PLQE and TRPL decays (Fig. 4c). We found that indeed, an increase in shallow defect density could not by itself recreate the severe decrease in PLQE and TRPL lifetime we observed without showing a very strong trap-filling feature in the first 10 ns of the TRPL decay (not observed in our experimental data). However, increasing the shallow defect density in addition to a 10^{15} cm^{-3} Bi trap density produced simulations that match the experimental TRPL decay shape better (Fig. 4c(i)). Hence, our simulations suggest that compensatory shallow defects contribute to recombination processes, but Bi/Sb defects determine overall non-radiative recombination rates. This evidence, together with the small barrier to recombination predicted by incorporation of the dopants is thermodynamically more favorable, suggest that the increased non-radiative recombination in of Bi- and Sb-doped films is mainly due to the direct trapping-recombination on the dopant sites. Encouragingly, this indicates that n-doping Sn-containing perovskites is not always doomed to increase non-radiative recombination, as the compensatory acceptor defects formed seem only minimally recombination-active.

2.3 Bi^{3+} impurities in perovskite precursor chemicals

The deleterious effect of very small amounts of Bi^{3+} doping (1 ppm) on the optoelectronic properties of lead–tin perovskites raises concerns about the potential presence of Bi^{3+} as an impurity in perovskite precursor chemicals. Even very high purity precursors normally only quote purity to 15 ppm and could thus have impurities on this scale (0.0001%). We tested a range of lead–tin perovskite precursor powders for Bi and Sb impurities by ICP-MS and were able to detect these elements to a sensitivity of 0.01 ppm. The type, supplier, and purity of each precursor we investigated is listed in Table S2 (ESI†), and the absolute Bi and Sb impurity densities determined by ICP-MS are presented in Table 2. These are representative of impurity concentrations that can be present under the typical operating conditions of a metal halide perovskite-producing laboratory, under which cross-contamination cannot be fully excluded. Even with strict fabrication procedures and cleanliness protocols, contamination may occur while precursor chemicals are stored in a glovebox area where Bi and Sb are also stored and occasionally handled. In addition, we emphasize that at such low impurity concentrations, batch-to-batch variation is likely

This journal is © The Royal Society of Chemistry 2025

J. Mater. Chem. C, 2025, **13**, 5161–5171 | **5167**

Table 2 Bi and Sb impurity concentrations in perovskite precursor chemicals, determined by ICP-MS

	Contaminant concentration (ppm)	
	Sb (mean ± stdev)	Bi (mean ± stdev)
FAI	0.580 ± 0.225	0.057 ± 0.059
CsI	0.356 ± 0.057	0.027 ± 0.017
PbI$_2$	0.025 ± 0.002	0.026 ± 0.005
SnI$_2$ (A)	$0.204^a \pm 0.008$	Not detected (<0.01)
SnI$_2$ (B)	$0.298^a \pm 0.002$	$1.059^a \pm 0.012$
SnF$_2$	$1.816^a \pm 0.047$	$1.613^a \pm 0.065$
Sn(0)	$0.476^a \pm 0.010$	$0.198^a \pm 0.002$

^{a} Signifies a minimum amount, as some solids remained after sample digestion which were deemed insoluble in nitric acid.

and hence this data is not necessarily representative of other batches of a certain material or supplier.

The concentration of Bi which each precursor chemical would deliver to the perovskite ink (a 1.8 M dispersion of FA$_{0.83}$Cs$_{0.17}$Pb$_{0.5}$Sn$_{0.5}$I$_3$ with 10% SnF$_2$ and 10 mg ml^{-1} Sn^0) is shown in Fig. 5a. In our case, no precursors contributed significant levels of Sb (>10 ppm), but one precursor contributed possibly significant levels of Bi (>0.1 ppm) to the solution. This was the SnI$_2$ precursor labelled 'B', at 0.5 ppm. However, when we fabricated perovskite films made using this SnI$_2$ and compared them to films made using an alternate SnI$_2$ precursor containing no detected Bi (labelled 'A'), we found no significant difference in PLQE (Fig. S7, ESI†). One possible explanation for this is that the Bi impurity could be present in its metallic neutral state within the precursor, since ICP-MS cannot determine in which oxidation state a trace impurity exists. Sn is more readily oxidized than Bi, so it is feasible that

Bi impurities remain in their neutral state during the synthesis of SnI$_2$. Bi^0 is not expected to become dissolved in the perovskite ink, as neither Pb^{2+} nor Sn^{2+} are expected to be able to oxidize it, and as such the presence of Bi^0 impurities in perovskite precursor chemicals is not expected to lead to Bi^{3+} doping of the perovskite.

Although not demonstrated to be significant in our case, Bi^{3+} impurities could certainly present a problem for the field of perovskite photovoltaics in general, particularly when large quantities of precursors are needed for scaling up. We propose a facile solution for removing Bi^{3+} impurities by treating the perovskite ink with a small amount of Sn^0 metal powder before filtering. Both Sn and Pb are more readily oxidized than Bi, which means that the following reaction is expected to take place between Sn^0 and Bi^{3+} (eqn (1)).

$$3Sn^0_{(s)} + 2Bi^{3+}_{(sol)} \Rightarrow 2Bi^0_{(s)} + 3Sn^{2+}_{(sol)} \tag{1}$$
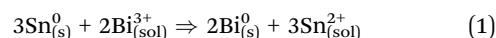
Bi^0 is subsequently expected to precipitate out of the solution and would be filtered out along with excess Sn^0. To test this approach, we prepared a precursor ink and doped it with a large amount of Bi^{3+} (100 ppm), which would ordinarily result in films with very low PLQE. This concentration of Bi^{3+} visibly colors the ink orange. We subsequently added 10 mg ml^{-1} Sn^0 powder to the solution and stirred it for 1 hour (Fig. 5b). During the first ~20 minutes, the orange color slowly disappeared until the original yellow color of the precursor ink was restored. We then filtered this precursor ink and used it to fabricate perovskite films. The PLQE (Fig. 5c) of these films was comparable to undoped perovskite films. This confirms that the addition of Sn^0 powder removes Bi^{3+} impurities from perovskite
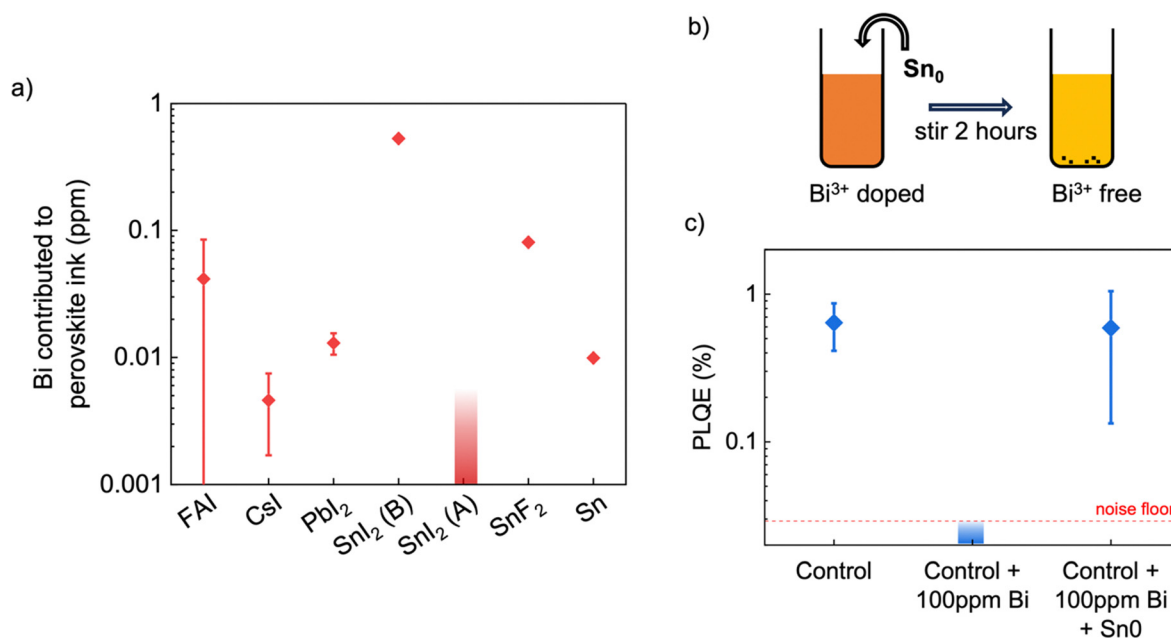
Fig. 5 (a) Bi density, in ppm with respect to combined Pb and Sn content, contributed to FA$_{0.83}$Cs$_{0.17}$Pb$_{0.5}$Sn$_{0.5}$I$_3$ perovskite precursor ink by commercial precursor chemicals, as determined by ICP-MS. (b) Schematic illustrating treatment of Bi^{3+}-containing perovskite precursor ink with Sn$_0$ powder to reduce and remove Bi^{3+}. (c) PLQE of lead–tin perovskite films without any Bi^{3+} doping, doped with 100 ppm Bi^{3+}, and doped with 100 ppm Bi^{3+} and subsequently treated with Sn^0 for 1 hour, showing complete recovery of PLQE after Sn^0 treatment.

5168 | J. Mater. Chem. C, 2025, **13**, 5161–5171

This journal is © The Royal Society of Chemistry 2025

precursor inks. For neat Pb perovskites, in theory Pb^0 powder can be added to achieve the same effect. Overall, we demonstrate that although Bi impurities can be present in perovskite precursors at significant concentrations, these can be easily removed by reduction of Bi in the precursor solution. We note that metallic Sn^0 is already a popular additive to tin-based perovskite inks, where it is said to reduce Sn^{4+} impurities in solution to Sn^{2+} *via* comproportionation, and thus improve device reproducibility and performance.[38] It may be the case that these improvements are also caused by the ability of metallic Sn^0 to purify precursor solutions from all metallic impurities which are less reactive than Sn.

3. Conclusion

In conclusion, we investigated the effect of Bi^{3+} and Sb^{3+} doping in lead–tin halide perovskite and demonstrated that both dopants strongly increase the rate of non-radiative recombination within the perovskite. Through DFT simulations, we have shown that Bi^{3+} and Sb^{3+} can be stably incorporated in the perovskite lattice in the substitutional position to Pb^{2+}, where they directly induce deep electron trap states within the band gap of the material. Ultimately, we conclude that the strong charge trapping activity of Bi^{3+} and Sb^{3+} makes them unsuitable for use as n-dopants in tin-based perovskites.

Our experiments showed that while lead–tin perovskites are more tolerant towards the presence of Sb^{3+} in the perovskite precursor, they are extremely sensitive to the incorporation of Bi^{3+}, showing quenched photoluminescence at concentrations as low as 1 ppm. We found that some precursors contribute bismuth concentrations approaching 0.5 ppm to the perovskite precursor ink but reveal that the use of these precursors did not result in films with significantly accelerated non-radiative recombination, possibly due to Bi impurities existing in their metallic rather than ionic form. However, these Bi^{3+} impurities can be easily removed from perovskite precursors by stirring with metallic Sn^0 powder. Using this method, we demonstrate the successful removal of 100 ppm Bi from our perovskite precursor such that the electronic quality of the resulting film is equal to that of undoped films.

This work demonstrates how very small impurity concentrations can strongly affect films quality and hence highlights the importance of precursor chemical purity. It also raises the need to screen potential perovskite dopants for the creation of potential trap states that lie within the perovskite bandgap, which may vary not only by dopant but also by perovskite composition.

Data availability

Data for this article are available at Oxford Research Archives at **https://dx.doi.org/10.5287/ora-kqdreg40y**.

Conflicts of interest

H. J. S. is co-founder and chief scientific officer of Oxford PV Ltd, a company commercializing perovskite PV technology.

Acknowledgements

References

1 M. A. Green, A. Ho-Baillie and H. J. Snaith, The Emergence of Perovskite Solar Cells, *Nat. Photonics*, 2014, **8**(7), 506–514, DOI: **10.1038/nphoton.2014.134**.

2 M. T. Klug, R. L. Milot, J. B. Patel, T. Green, H. C. Sansom, M. D. Farrar, A. J. Ramadan, S. Martani, Z. Wang, B. Wenger, J. M. Ball, L. Langshaw, A. Petrozza, M. B. Johnston, L. M. Herz and H. J. Snaith, Metal Composition Influences Optoelectronic Quality in Mixed-Metal Lead–Tin Triiodide Perovskite Solar Absorbers, *Energy Environ. Sci.*, 2020, **13**(6), 1776–1787, DOI: **10.1039/D0EE00132E**.

3 K. J. Savill, A. M. Ulatowski and L. M. Herz, Optoelectronic Properties of Tin–Lead Halide Perovskites, *ACS Energy Lett.*, 2021, **6**(7), 2413–2426, DOI: **10.1021/acsenergylett.1c00776**.

4 M. T. Hörantner, T. Leijtens, M. E. Ziffer, G. E. Eperon, M. G. Christoforo, M. D. McGehee and H. J. Snaith, The Potential of Multijunction Perovskite Solar Cells, *ACS Energy Lett.*, 2017, **2**(10), 2506–2513, DOI: **10.1021/acsenergylett.7b00647**.

5 C. C. Stoumpos, C. D. Malliakas and M. G. Kanatzidis, Semiconducting Tin and Lead Iodide Perovskites with Organic Cations: Phase Transitions, High Mobilities, and Near-Infrared Photoluminescent Properties, *Inorg. Chem.*, 2013, **52**(15), 9019–9038, DOI: **10.1021/ic401215x**.

6 J. Thiesbrummel, V. M. Le Corre, F. Peña-Camargo, L. Perdigón-Toro, F. Lang, F. Yang, M. Grischek, E. Gutierrez-Partida, J. Warby, M. D. Farrar, S. Mahesh, P. Caprioglio, S. Albrecht, D. Neher, H. J. Snaith and M. Stolterfoht, Universal Current Losses in Perovskite Solar Cells Due to Mobile Ions, *Adv. Energy Mater.*, 2021, 2101447, DOI: **10.1002/aenm.202101447**.

7 K. J. Savill, A. M. Ulatowski, M. D. Farrar, M. B. Johnston, H. J. Snaith and L. M. Herz, Impact of Tin Fluoride Additive on the Properties of Mixed Tin–Lead Iodide Perovskite

This journal is © The Royal Society of Chemistry 2025

J. Mater. Chem. C, 2025, **13**, 5161–5171 | **5169**

Semiconductors, *Adv. Funct. Mater.*, 2020, **30**(52), 2005594, DOI: **10.1002/adfm.202005594**.

8 D. Meggiolaro, D. Ricciarelli, A. A. Alasmari, F. A. S. Alasmary and F. De Angelis, Tin versus Lead Redox Chemistry Modulates Charge Trapping and Self-Doping in Tin/Lead Iodide Perovskites, *J. Phys. Chem. Lett.*, 2020, **11**(9), 3546–3556, DOI: **10.1021/acs.jpclett.0c00725**.

9 D. Ricciarelli, D. Meggiolaro, F. Ambrosio and F. De Angelis, Instability of Tin Iodide Perovskites: Bulk p-Doping versus Surface Tin Oxidation, *ACS Energy Lett.*, 2020, **5**(9), 2787–2795, DOI: **10.1021/acsenergylett.0c01174**.

10 F. Pena-Camargo, J. Thiesbrummel, H. Hempel, A. Musiienko, V. M. L. Corre, J. Diekmann, J. Warby, T. Unold, F. Lang, D. Neher and M. Stolterfoht, Revealing the Doping Density in Perovskite Solar Cells and Its Impact on Device Performance, *Appl. Phys. Rev.*, 2022, **9**, 021409.

11 R. L. Milot, G. E. Eperon, T. Green, H. J. Snaith, M. B. Johnston and L. M. Herz, Radiative Monomolecular Recombination Boosts Amplified Spontaneous Emission in HC(NH$_2$)$_2$SnI$_3$ Perovskite Films, *J. Phys. Chem. Lett.*, 2016, **7**(20), 4178–4184, DOI: **10.1021/acs.jpclett.6b02030**.

12 R. L. Milot, M. T. Klug, C. L. Davies, Z. Wang, H. Kraus, H. J. Snaith, M. B. Johnston and L. M. Herz, The Effects of Doping Density and Temperature on the Optoelectronic Properties of Formamidinium Tin Triiodide Thin Films, *Adv. Mater.*, 2018, **30**(44), 1804506, DOI: **10.1002/adma.201804506**.

13 R. Lin, K. Xiao, Z. Qin, Q. Han, C. Zhang, M. Wei, M. I. Saidaminov, Y. Gao, J. Xu, M. Xiao, A. Li, J. Zhu, E. H. Sargent and H. Tan, Monolithic All-Perovskite Tandem Solar Cells with 24.8% Efficiency Exploiting Comproportionation to Suppress Sn(II) Oxidation in Precursor Ink, *Nat. Energy*, 2019, **4**(10), 864–873, DOI: **10.1038/s41560-019-0466-3**.

14 J. Euvrard, Y. Yan and D. B. Mitzi, Electrical Doping in Halide Perovskites, *Nat. Rev. Mater.*, 2021, **6**(6), 531–549, DOI: **10.1038/s41578-021-00286-z**.

15 F. P. Sabino, A. Zunger and G. M. Dalpian, Intrinsic Doping Limitations in Inorganic Lead Halide Perovskites, *Mater. Horiz.*, 2022, **9**(2), 791–803, DOI: **10.1039/D1MH01371H**.

16 R. Shi and R. Long, Atomic Model for Alkali Metal-Doped Tin–Lead Mixed Perovskites: Insight from Quantum Dynamics, *J. Phys. Chem. Lett.*, 2023, **14**(11), 2878–2885, DOI: **10.1021/acs.jpclett.3c00602**.

17 F. Liu, J. Jiang, Y. Zhang, C. Ding, T. Toyoda, S. Hayase, R. Wang, S. Tao and Q. Shen, Near-Infrared Emission from Tin–Lead (Sn–Pb) Alloyed Perovskite Quantum Dots by Sodium Doping, *Angew. Chem., Int. Ed.*, 2020, **59**(22), 8421–8424, DOI: **10.1002/anie.201916020**.

18 Z. Chang, D. Zheng, S. Zhao, L. Wang, S. Wu, L. Liu, Z. Li, L. Zhang, Q. Dong, H. Wang, S. Wang, K. Wang and S. (Frank) Liu, Designing Heterovalent Substitution with Antioxidant Attribute for High-Performance Sn–Pb Alloyed Perovskite Solar Cells, *Adv. Funct. Mater.*, 2023, **33**(22), 2214983, DOI: **10.1002/adfm.202214983**.

19 C. Park, J. Choi, J. Min and K. Cho, Suppression of Oxidative Degradation of Tin–Lead Hybrid Organometal Halide Perovskite Solar Cells by Ag Doping, *ACS Energy Lett.*, 2020, **5**(10), 3285–3294, DOI: **10.1021/acsenergylett.0c01648**.

20 S. R. Sahamir, M. A. Kamarudin, T. S. Ripolles, A. K. Baranwal, G. Kapil, Q. Shen, H. Segawa, J. Bisquert and S. Hayase, Enhancing the Electronic Properties and Stability of High-Efficiency Tin–Lead Mixed Halide Perovskite Solar Cells via Doping Engineering, *J. Phys. Chem. Lett.*, 2022, **13**(13), 3130–3137, DOI: **10.1021/acs.jpclett.2c00699**.

21 B. Chen, Z. Yu, A. Onno, Z. Yu, S. Chen, J. Wang, Z. C. Holman and J. Huang, Bifacial All-Perovskite Tandem Solar Cells, *Sci. Adv.*, 2022, **8**(47), eadd0377, DOI: **10.1126/sciadv.add0377**.

22 A. L. Abdelhady, M. I. Saidaminov, B. Murali, V. Adinolfi, O. Voznyy, K. Katsiev, E. Alarousu, R. Comin, I. Dursun, L. Sinatra, E. H. Sargent, O. F. Mohammed and O. M. Bakr, Heterovalent Dopant Incorporation for Bandgap and Type Engineering of Perovskite Crystals, *J. Phys. Chem. Lett.*, 2016, **7**(2), 295–301, DOI: **10.1021/acs.jpclett.5b02681**.

23 K. Kobayashi, H. Hasegawa, Y. Takahashi, J. Harada and T. Inabe, Electronic Properties of Tin Iodide Hybrid Perovskites: Effect of Indium Doping, *Mater. Chem. Front.*, 2018, **2**(7), 1291–1295, DOI: **10.1039/C7QM00587C**.

24 E. Mosconi, B. Merabet, D. Meggiolaro, A. Zaoui and F. De Angelis, First-Principles Modeling of Bismuth Doping in the MAPbI$_3$ Perovskite, *J. Phys. Chem. C*, 2018, **122**(25), 14107–14112, DOI: **10.1021/acs.jpcc.8b01307**.

25 J. L. Lyons, Effective Donor Dopants for Lead Halide Perovskites, *Chem. Mater.*, 2021, **33**(15), 6200–6205, DOI: **10.1021/acs.chemmater.1c01898**.

26 M. Yavari, F. Ebadi, S. Meloni, Z. S. Wang, T. C.-J. Yang, S. Sun, H. Schwartz, Z. Wang, B. Niesen, J. Durantini, P. Rieder, K. Tvingstedt, T. Buonassisi, W. C. H. Choy, A. Filippetti, T. Dittrich, S. Olthof, J.-P. Correa-Baena and W. Tress, How Far Does the Defect Tolerance of Lead-Halide Perovskites Range? The Example of Bi Impurities Introducing Efficient Recombination Centers, *J. Mater. Chem. A*, 2019, **7**(41), 23838–23853, DOI: **10.1039/C9TA01744E**.

27 A. M. Ulatowski, A. D. Wright, B. Wenger, L. R. V. Buizza, S. G. Motti, H. J. Eggimann, K. J. Savill, J. Borchert, H. J. Snaith, M. B. Johnston and L. M. Herz, Charge-Carrier Trapping Dynamics in Bismuth-Doped Thin Films of MAPbBr$_3$ Perovskite. *J. Phys, Chem. Lett.*, 2020, **11**(9), 3681–3688, DOI: **10.1021/acs.jpclett.0c01048**.

28 P. K. Nayak, M. Sendner, B. Wenger, Z. Wang, K. Sharma, A. J. Ramadan, R. Lovrinčić, A. Pucci, P. K. Madhu and H. J. Snaith, Impact of Bi^{3+} Heterovalent Doping in Organic–Inorganic Metal Halide Perovskite Crystals, *J. Am. Chem. Soc.*, 2018, **140**(2), 574–577, DOI: **10.1021/jacs.7b11125**.

29 R. Meng, G. Wu, J. Zhou, H. Zhou, H. Fang, M. A. Loi and Y. Zhang, Understanding the Impact of Bismuth Heterovalent Doping on the Structural and Photophysical Properties of CH$_3$NH$_3$PbBr$_3$ Halide Perovskite Crystals with Near-IR Photoluminescence, *Chem. – Eur. J.*, 2019, **25**(21), 5480–5488, DOI: **10.1002/chem.201805370**.

30 L. Gregori, D. Meggiolaro and F. De Angelis, Combining Trivalent Ion-Doping with Halide Alloying to Increase the Efficiency of Tin Perovskites, *Small*, 2024, 2403413, DOI: **10.1002/smll.202403413**.

5170 | *J. Mater. Chem. C*, 2025, **13**, 5161–5171

This journal is © The Royal Society of Chemistry 2025

31 L. Huang, S. Bu, D. Zhang, R. Peng, Q. Wei, Z. Ge and J. Zhang, Schottky/P-n Cascade Heterojunction Constructed by Intentional n-Type Doping Perovskite Toward Efficient Electron Layer-Free Perovskite Solar Cells, *Sol. RRL*, 2019, **3**(2), 1800274, DOI: **10.1002/solr.201800274**.

32 J. R. Palmer, J. Yang, A. Gupta, C. J. Dolan, B. W. Larson, S. P. Dunfield, A. Mannodi-Kanakkithodi and D. P. Fenning, Bismuth in Lead–Tin Alloy Perovskites: Effect on Material Properties and Photovoltaic Device Performance, *ACS Appl. Energy Mater.*, 2024, **7**(7), 2726–2734, DOI: **10.1021/acsaem.3c03156**.

33 S. Zeiske, C. Kaiser, P. Meredith and A. Armin, Sensitivity of Sub-Bandgap External Quantum Efficiency Measurements of Solar Cells under Electrical and Light Bias, *ACS Photonics*, 2020, **7**(1), 256–264, DOI: **10.1021/acsphotonics.9b01531**.

34 J. P. Perdew, K. Burke and M. Ernzerhof, Generalized Gradient Approximation Made Simple, *Phys. Rev. Lett.*, 1996, **77**(18), 3865–3868, DOI: **10.1103/PhysRevLett.77.3865**.

35 J. P. Perdew, M. Ernzerhof and K. Burke, Rationale for Mixing Exact Exchange with Density Functional Approximations, *J. Chem. Phys.*, 1996, **105**(22), 9982–9985, DOI: **10.1063/1.472933**.

36 C. Adamo and V. Barone, Toward Reliable Density Functional Methods without Adjustable Parameters: The PBE0 Model, *J. Chem. Phys.*, 1999, **110**(13), 6158–6170, DOI: **10.1063/1.478522**.

37 X. Zhang, J.-X. Shen, M. E. Turiansky and C. G. Van De Walle, Hidden Role of Bi Incorporation in Nonradiative Recombination in Methylammonium Lead Iodide, *J. Mater. Chem. A*, 2020, **8**(26), 12964–12967, DOI: **10.1039/D0TA04968A**.

38 T. Nakamura, S. Yakumaru, M. A. Truong, K. Kim, J. Liu, S. Hu, K. Otsuka, R. Hashimoto, R. Murdey, T. Sasamori, H. D. Kim, H. Ohkita, T. Handa, Y. Kanemitsu and A. Wakamiya, Sn(ɪᴠ)-Free Tin Perovskite Films Realized by in Situ Sn(0) Nanoparticle Treatment of the Precursor Solution, *Nat. Commun.*, 2020, **11**(1), 3008, DOI: **10.1038/s41467-020-16726-3**.

This journal is © The Royal Society of Chemistry 2025

J. Mater. Chem. C, 2025, **13**, 5161–5171 | **5171**